

First mixed-metal imidazoles containing alkali and alkaline earth metals: mechanochemical synthesis and crystal structure of $AMgIm_3$ (A=Na, K)

Sanja Burazer,[†] Fabrice Morelle,[#] Yaroslav Filinchuk,[#] Radovan Černý,[‡] Jasminka Popović^{*†}

[†] Laboratory for Synthesis and Crystallography of Functional Materials, Division for Materials Physics, Ruđer Bošković Institute, Bijenička 54, HR-10000 Zagreb, Croatia

[#] SST/IMCN/MOST – Molecules, Solids and Reactivity, Université catholique de Louvain, Place de l'Université 1, 1348 Ottignies-Louvain-la-Neuve, Belgium

[‡] Laboratory of Crystallography, DQMP, University of Geneva, Quai Ernest-Ansermet 24, CH-1211 Geneva, Switzerland

Abstract: First bimetallic imidazoles containing alkali and alkaline earth metals, $NaMgIm_3$ and $KMgIm_3$, prepared by mechanochemical synthesis, and reported in this paper. $NaMgIm_3$ has been prepared by the reaction between $NaIm$ and $Mg(BH_4)_2$ as well as directly from $NaIm$ and $MgIm_2$. Structural evolution and thermal stability was followed by *in-situ* high temperature XRPD experiment utilizing synchrotron radiation. In both compounds, the imidazolate ligand is connected to four metal cations forming a complex 3D network with channels running along the *c*-direction. $NaMgIm_3$ and $KMgIm_3$ are the first members of new family of imidazolate frameworks with *stp* topology. Formation of mixed alkali metal imidazolate compounds is thermodynamically controlled: $LiIm$ and $MgIm_2$ have not yielded a mixed-metal compound while KIm reacts swiftly and forms $KMgIm_3$.

INTRODUCTION

Materials research over last decades has been focused on providing novel platforms which would enable effective solutions for increasing energy demands of today's society, where hydrogen is set as a key element within the quest for sustainable alternatives.¹ Different crystalline and/or porous systems have been considered as a material-of-choice for hydrogen storage, among which metal borohydrides, exhibiting a high gravimetric and volumetric hydrogen density, represent a very promising class of compounds where hydrogen is covalently bonded to a light element, forming a complex BH_4^- anions. A comprehensive review on the structural versatility and storage properties of different mono-, bi- and tri-metallic borohydrides is given in ². The tetrahedral BH_4^- anion is directional bridging ligand, coordinating metal cations preferably *via* its edges, as evidenced in the case of porous γ - $Mg(BH_4)_2$.³ Additionally, metal-organic frameworks (MOFs), and its subclass zeolitic imidazolate frameworks (ZIFs), have also been most extensively studied as a media where hydrogen can be physisorbed in molecular form within the nanopores.^{4, 5} Although some MOFs

are known to possess high hydrogen storage capacities those are usually achieved only at extreme conditions such as low temperatures (77 K) as in case of MOF-505.⁶

Initial intention of our research was to explore the possibility of a coalescence between the class of borohydrides and imidazolates, which would result in the formation of coordination frameworks involving complex hydride anions as ligands. Coordinatively active anions, imidazolates, would serve as a structural unit of the framework while borohydride anions could provide functionality. Imidazolates can act as a bridging anionic ligands thus allowing various connectivity and structural topologies of the resulting frameworks. Moreover, the feasibility of this idea relies upon the fact that metal-imidazole-metal bond angle of 145° is very similar to metal-borohydride-metal angle observed, for example, in $\text{Mg}(\text{BH}_4)_2$.⁷ The proof of the concept can be illustrated by the synthesis of the first mixed anion borohydride imidazolate, Li_2ImBH_4 .⁸ However, contrary to our expectation, the mechanochemical reaction between $\text{Mg}(\text{BH}_4)_2$ and NaIm have not yielded a hybrid material containing both directional ligands, yet it resulted in the formation of new type of bimetallic imidazolate, NaMgIm_3 . Although imidazolates have rich and versatile coordination potential, especially highlighted in ^{9, 10}, bimetallic imidazolates are extremely scarce in literature. Among few, the 2D grid-shaped coordination polymer $[\text{Co}^{\text{II}}\text{Cu}^{\text{I}}_2(\text{Im})_4]$ has been reported.¹¹ Asymmetric unit contains tetrahedrally coordinated cobalt(II) atom and linearly coordinated copper(I) ion where metal centers are bridged by a deprotonated imidazole molecule. An interesting structure has been revealed for Cu_2ZnIm_6 , exhibiting a network of alternating zinc and copper atoms bridged by imidazolate moieties, with the copper and zinc atoms surrounded by two and four imidazolate nitrogen atoms, respectively.¹² It is notable that the Cu(I)-Im-Zn(II) bridge found in this compound is analogous to those found in copper-zinc superoxide dismutase metalloenzymes.¹³ Furthermore, recently it has been demonstrated that zeolitic imidazolate frameworks are not restricted to exclusively tetrahedral nets, as in the first example of an imidazolate based on a bimetallic coordination net, $\text{In}_2\text{Zn}_3(\text{Im})_{12}$ with In(III) in octahedral coordination environment.⁹ This structure has the topology of the $\text{Al}_2\text{Si}_3\text{O}_{12}$ part of a garnet and provide the illustration on an extraordinarily rich chemistry awaiting systematic exploration of imidazolates. Nice example where bimetallic imidazolate shows great dynamic uptake selectivity for CO_2 over methane under wet conditions is reported in ¹⁴. While those few examples of bimetallic imidazolates can be found in the literature in the case of transition metal atoms, there are no reports on mixed metal imidazolates involving alkali and earth alkali metals. It is shown that alkali imidazolates (NaIm , KIm and LiIm) form the dense and hypercoordinated structures where the coordinative demand of the metal cation increases with an increase of the ionic radii. The Li^+ cation exhibits a strong propensity to form heteroleptic structures, while the K^+ cation allows to coordinate the Im ring through the π -system.¹⁵ On the other hand, the utilization of an alkali earth metal led to formation of porous zeolitic imidazolate framework in the case of magnesium imidazolate (MgIm_2).^{15, 16} To the best of our knowledge, only transition metals were used as metal centres in bimetallic imidazolates and this is the first time bimetallic imidazolates contain both alkali and alkaline earth metals.

EXPERIMENTAL SECTION

Synthesis

Four mechanochemical reactions between $\text{Mg}(\text{BH}_4)_2$ or MgIm_2 and AIm ($\text{A} = \text{Na}, \text{K}, \text{Li}$) were conducted using the Planetary Micro Mill Fritsch Pulverisette 7 premium line. The reactants and stainless steel balls ($d = 5$ mm) were loaded in a stainless steel vial (25 ml) under inert conditions. In each synthesis the balls-to-sample mass ratio amounted to 25:1. Ball milling was performed at 550 rpm for 10 min, followed by a 5 min rest time; this procedure was repeated 12 times. The reactants and molar ratios used are given in Table 1.

Table 1. Reactants used for the mechanochemical synthesis.

	Reactants and molar ratio
S1	$\text{Mg}(\text{BH}_4)_2$ and $\text{NaIm} = 1:6$
S2	MgIm_2 and $\text{NaIm} = 1:2$
S3	MgIm_2 and $\text{KIm} = 1:2$
S4	MgIm_2 and $\text{LiIm} = 1:2$

Anhydrous magnesium borohydride, $\text{Mg}(\text{BH}_4)_2$ (99.99%) was purchased from Sigma-Aldrich while the imidazoles were prepared by the procedure reported elsewhere.¹⁵ All handling and manipulation of the chemicals was performed in argon-filled glovebox.

X-ray powder diffraction (XRPD) at RT

XRPD measurements at room temperature (RT) were performed using a Stoe IPDS-P diffractometer with monochromated $\text{CuK}\alpha 1$ radiation ($\lambda = 1.54060 \text{ \AA}$) and a curved image plate detector, in Debye-Scherrer geometry. Air-sensitive samples were mounted in a glovebox in 0.8 borosilicate capillaries sealed with vacuum grease. Data was collected at RT, in 2θ range: $2-100^\circ$ with counting time of 40 s/step. XRPD patterns are shown on Figures S1-S4.

Synchrotron radiation X-ray powder diffraction (SR-XRPD) at HT

High temperature *in-situ* powder diffraction (HT-XRPD) data were collected at the beamline BM01, SNBL at the ESRF, Grenoble, France. The samples were mounted in 0.5 mm borosilicate capillaries and closed with vacuum grease. Measurement parameters are: $\lambda_{\text{S1}}=0.8187 \text{ \AA}$, $\lambda_{\text{S2}, \text{S3}, \text{S4}}=0.7149 \text{ \AA}$, sample rotation $0-40^\circ$, X-ray exposure time 40 s. The Dectris Pilatus 2M detector was used for recording 2D powder data at the sample to detector distances of 200 or 400 mm. Samples were heated in the temperature range from RT to 400°C (with heating rate $5^\circ\text{C}/\text{min}$) by a heat blower. 2D images were integrated and treated with local program Bubble.¹⁷

Structure solution, analysis and validation

Crystal structures of new compounds were solved and refined from the SR-PXD data. Indexing, space group determination as well as structure solution was carried out using FOX program.¹⁸

Structural model was refined by Rietveld method using the Fullprof program.¹⁹ The imidazolate anion was treated as a rigid body and only its position and orientation in the unit cell was varied.

The topology analysis of the underlying net in the novel crystal structures was done with the help of the program TOPOS.²⁰

Bond valence sum (BVS) is used for validation of the obtained structural models. Crystallographic positions, as determined by XRPD were used for BVS calculation. Soft bond valence parameters R_{ij} and b are taken from the literature.²¹ Results received from most commonly adopted empirical expression for the variation of the length d_{ij} of a bond with valence $v_{ij} = \exp[(R_{ij} - d_{ij})/b]$, were summed up to get the sum of all the valences from a given atom. Program VESTA was used for visualization of crystal structures.²²

RESULTS AND DISCUSSION

Phase analysis using HT SR-XRPD data

Diffraction patterns of as-milled products obtained after the mechanochemical reaction between $\text{Mg}(\text{BH}_4)_2$ and NaIm , as well as in-high temperature data, are shown in Fig 1a. It can be seen that as-milled sample S1 contains unreacted NaIm and significant amount of amorphous phase(s). At $T=118^\circ\text{C}$, new crystalline phase - NaMgIm_3 - starts to appear (Figure 1b). With further thermal treatment the peaks of NaIm disappear at $T=209^\circ\text{C}$. Simultaneously, another unknown crystalline phase starts to crystallize. As this unknown phase coexists together with NaMgIm_3 , significant overlap of diffraction peaks prevented its successful structure solution. Moreover this compound is stable in very narrow temperature range, from 209°C to 218°C . However, additional experiments were conducted and it was found that the new phase corresponds to high temperature polymorph of NaIm .²³ Above $T=218^\circ\text{C}$, only NaMgIm_3 diffraction peaks are present. The compound stays stable up to 340°C .

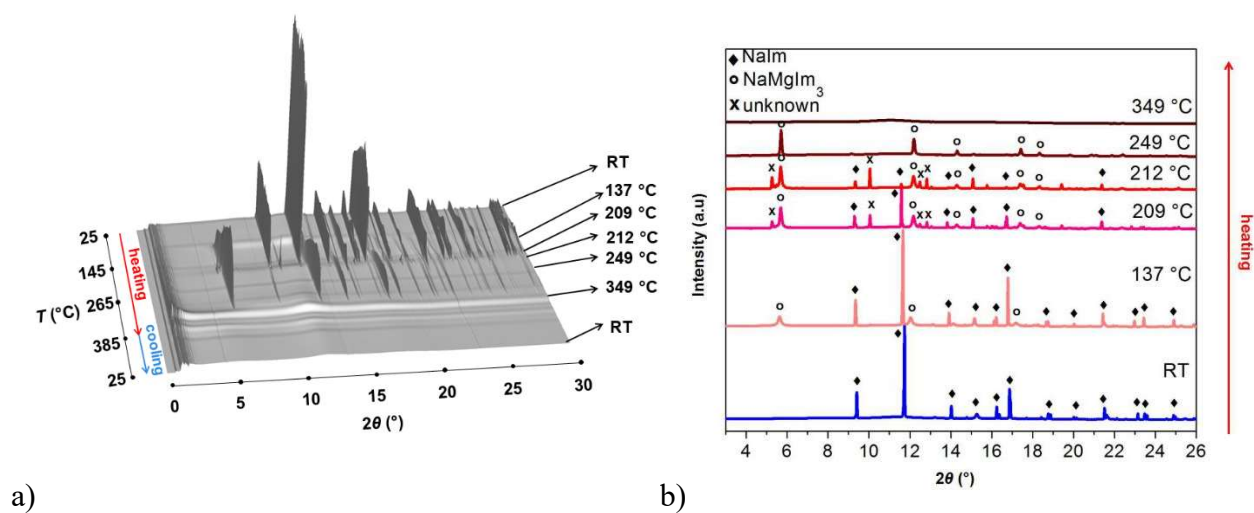


Figure 1. a) T-ramp of sample S1. b) Phase analysis of sample S1 T-ramp. Diffraction lines of NaIm are marked with diamonds, NaMgIm₃ phase with circles while the unknown phase is denoted with x.

Additional mechanochemical synthesis was conducted, starting from MgIm₂ and NaIm, in order to prepare pure NaMgIm₃ and to gain the further insight into its structural evolution and thermal stability. Diffraction patterns of as-milled products obtained after the mechanochemical reaction as well as in-high temperature data, are shown in Figure 2.

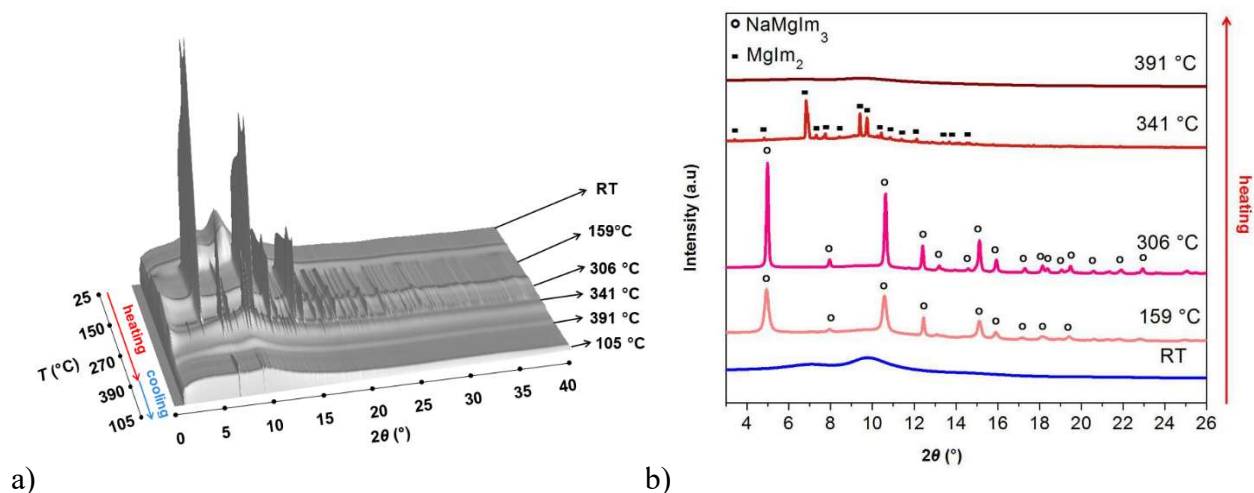


Figure 2. a) T-ramp of sample S2. b) Phase analysis of sample S2 T-ramp. Diffraction lines belonging to NaMgIm₃ phase are marked with circles and the diffraction lines belonging to MgIm₂ phase with squares.

As can be seen from Figure 2, as-milled sample S2 is amorphous up to $T=149^\circ\text{C}$ when NaMgIm₃ starts to crystallize. It remains stable up to 310°C . At $T=310^\circ\text{C}$ the diffraction lines of NaMgIm₃ disappear and MgIm₂ starts to crystallize. Magnesium imidazolate was stable up to 366°C . Interestingly, one can notice that NaMgIm₃ displays wider range of thermal stability ($118\text{-}340^\circ\text{C}$) when borohydride is present in the system.

Since the mechanochemical reaction between MgIm₂ and NaIm yielded a novel bimetallic imidazolate compound, further attempts have been made to prepare novel mixed metal imidazolates containing K and Li instead of Na. Diffraction patterns of as-milled products obtained after the mechanochemical reaction between MgIm₂ and KIm (S3), as well as *in-situ* high temperature measurements, are shown in Fig 3.

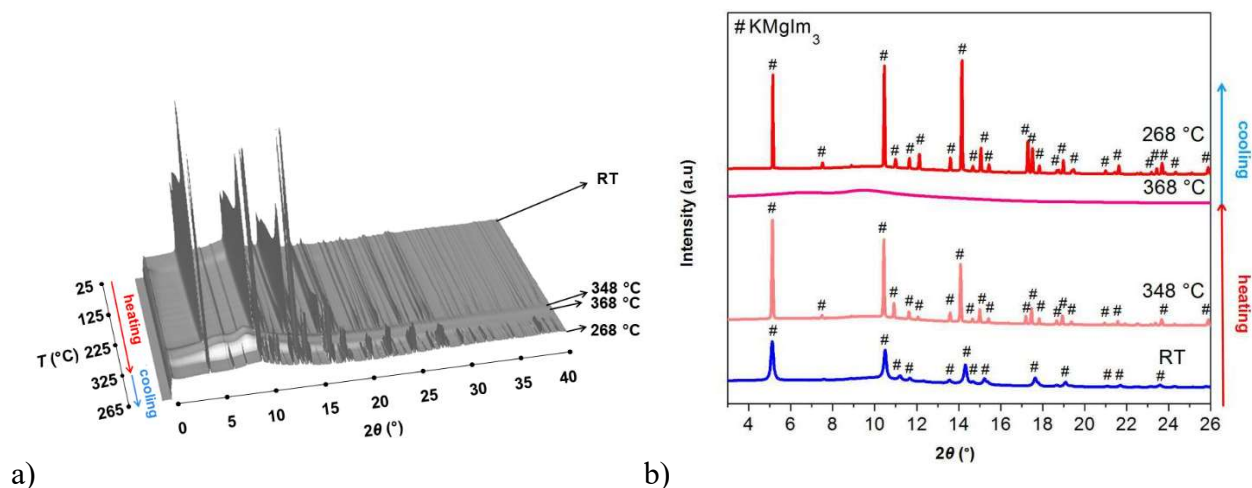


Figure 3. (a) T-ramp of sample S3. (b) Phase analysis of sample S3 T-ramp. Ladders are denoting the diffraction lines of KMgIm_3 phase.

In the case of KIm , unlike with NaIm , already the grinding without any thermal treatment proved to be sufficient for the formation of mixed metal imidazolate phase, KMgIm_3 . This compound is stable in a wide temperature range, from RT to 353°C, when it melts. Same compound recrystallizes below 298°C during cooling. Crystal structure of KMgIm_3 has also been solved from powder X-ray diffraction data.

When LiIm was used as a reactant in mechanochemical reaction with MgIm_2 , the milled sample at RT shows only amorphous halo (Figure 4). Diffraction lines of LiIm , start to appear at $T= 149^\circ\text{C}$ and the second reactant, MgIm_2 , starts to crystallize at $T= 185^\circ\text{C}$. Both compounds remained stable up to 296°C. No formation of mixed metal imidazolate was observed.

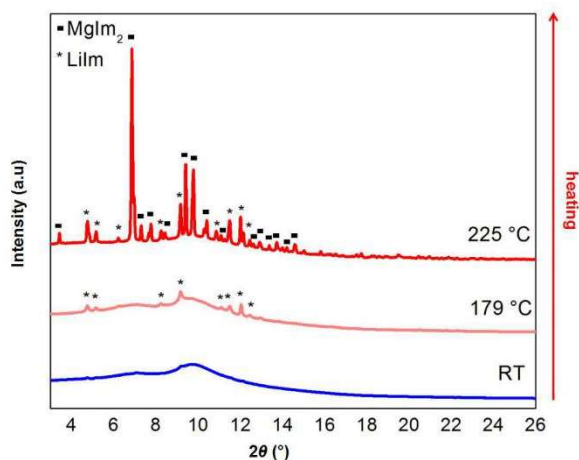


Figure 4. Phase analysis of Li sample T-ramp. Squares are denoting the diffraction lines of MgIm_2 phase and asterisks are denoting the diffraction lines of the LiIm phase.

Crystal structure of $AMgIm_3$ ($A = Na$ and K)

The crystal structure of $NaMgIm_3$ was solved using the diffraction data of the sample S1 at 262 °C and of the sample S3 at 333 °C. The selected diffraction peaks were indexed in a hexagonal cell. For structure solution, positions of one Na, one Mg atom and one imidazolate group for $NaMgIm_3$ and positions of one K, one Mg atom and one imidazolate group for $KMgIm_3$ were varied using corresponding antibump restraints. Rietveld plot from the refinement of $NaMgIm_3$ is given in Fig 5a and the crystal structure is shown in Fig 5b and c. The compound crystallizes in hexagonal system (space group $P6_322$). Crystal data for $NaMgIm_3$ and summary of structure refinement are listed in Table 2.

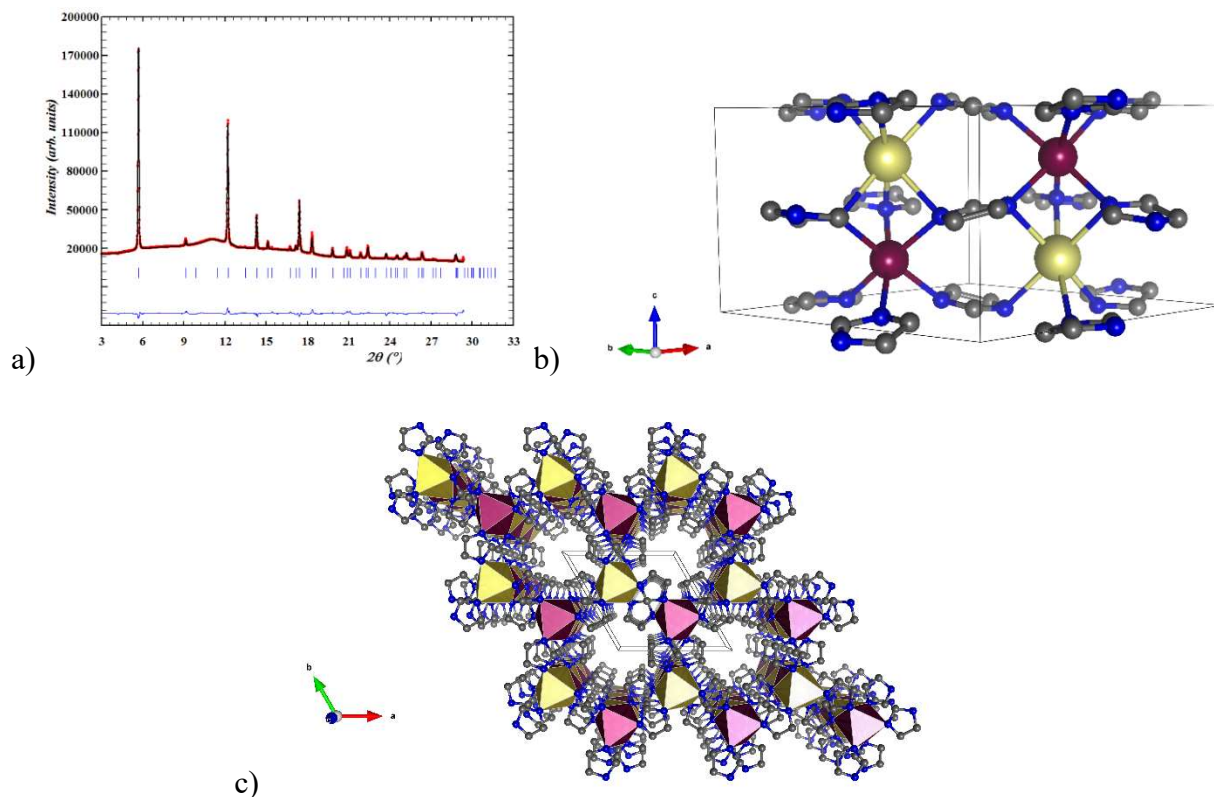


Figure 5. (a) Rietveld refinement of $NaMgIm_3$. Experimental pattern is given as red dots, black curve shows calculated profile and the difference curve is given blue. Vertical marks represent Bragg reflection of $NaMgIm_3$ (b) Crystal structure of $NaMgIm_3$; magnesium atoms are shown as purple balls, sodium is given in yellow, carbon is grey while nitrogen is shown in blue colour. (c) Extended crystal packing of $NaMgIm_3$ showing channels along c -direction.

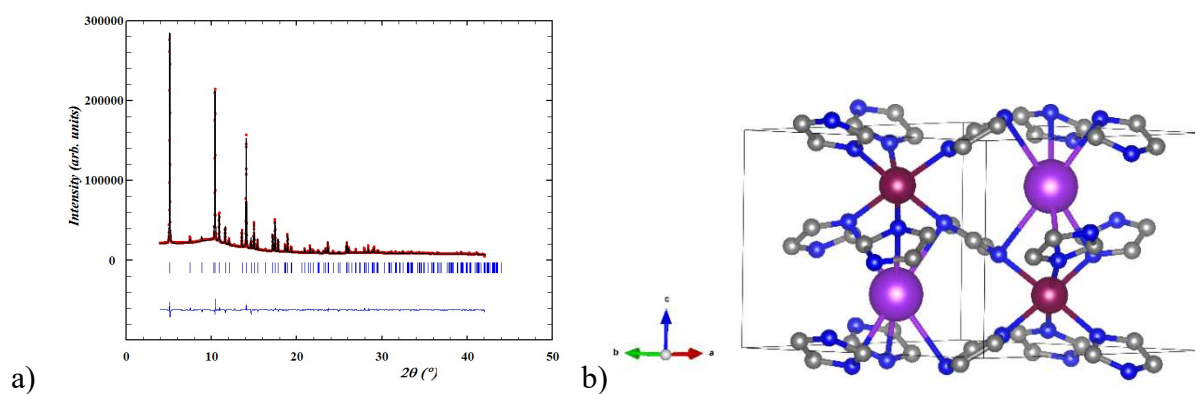
Table 2. Crystal data and summary of structure refinement for $NaMgIm_3$ and $KMgIm_3$

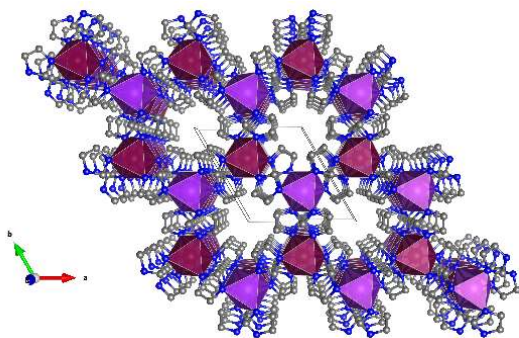
	$NaMgIm_3$	$KMgIm_3$
Profile function	Pseudo Voight	Pseudo Voight
R (profile)/ %	16.9	11.8
R (weighted profile)/ %	10.7	10.9

χ^2	$7.01 \cdot 10^3$	$8.03 \cdot 10^4$
Space group	P6 ₃ 22	P6 ₃ 22
a/ Å	9.50543(4)	9.22627(7)
c/ Å	6.57611(4)	7.50902(9)

Unlike monometallic imidazolates (NaIm and MgIm₂) which show tetrahedral coordination of metals¹⁴, in NaMgIm₃ both Na and Mg cation are exhibiting distorted octahedral coordination. The interatomic distances, $d(\text{M-N}_{\text{im}})$, are found to be longer in case of mixed metal imidazolates, as expected for a higher coordination number, compared to tetrahedrally coordinated metals cations in the case of NaIm and MgIm₂ ($d(\text{Na-N})_{\text{tet}}=2.4029$ Å, $d(\text{Na-N})_{\text{oct}}=2.5851$ Å; $d(\text{Mg-N})_{\text{tet}}=2.0410$ Å, $d(\text{Mg-N})_{\text{oct}}=2.3701$ Å). Same as in NaIm, imidazolate ligand is connected to 4 metal cations, where each N atom from imidazolate anion is coordinated with 2 cations forming a complex 3D network. Along the *c*-direction, Na and Mg are connected *via* bridging N atoms from three imidazole rings forming the chain of face-shared metal octahedra. Those chains along *c*-direction are mutually connected in an imidazole-bridged fashion, forming a zig-zag net in the *ab* plane. Crystal packing also displays there are channels running along the *c*-direction, located on the six-folded screw axis, as shown in Figure 5c. Channel is defined by the diameter $d \sim 6.6$ Å and the empty volume calculated from contact surface amounts to 28.5 Å³ (assuming the spherical probe of $r=1.4$ Å).

It was found that crystal structure of KMgIm₃ is similar to its sodium derivative (Figure 6b). Rietveld refinement is given in Figure 6a. Crystal data for both NaMgIm₃ and KMgIm₃, together with summary of structure refinement, are listed in Table 2.





c)

Figure 6. (a) Rietveld refinement of KMgIm_3 . Experimental pattern is given as red dots, black curve shows calculated profile and the difference curve is given blue. Vertical marks represent Bragg reflection of NaMgIm_3 (b) Crystal structure of KMgIm_3 ; magnesium atoms are shown as purple balls, potassium is given in violet, carbon is grey while nitrogen is shown in blue colour. (c) Extended crystal packing of NaMgIm_3 showing channels along c -direction.

Main difference between crystal structures of NaMgIm_3 and KMgIm_3 is related to the orientation of imidazolate rings. Although the imidazolate rings in the case of sodium compound deviate slightly from an ideal planar configuration, the rings can be considered as almost parallel to the ab plane, which is not the case for the potassium compound. Additionally, the two compounds show different degree of polyhedral deformation around the alkali metal cation; pronounced distortion of octahedra around sodium can be observed [$\angle(\text{N}_{\text{ax}}\text{-Na}\text{-N}_{\text{eq}})=76.65^\circ$], compared to the octahedra surrounding the potassium center [$\angle(\text{N}_{\text{ax}}\text{-K}\text{-N}_{\text{eq}})=84.45^\circ$].

According to BVS calculations, in NaMgIm_3 the valence sums for magnesium and sodium cations amount to 1.5 and 1, respectively. In the case of KMgIm_3 , the valence sums for magnesium and potassium are 1.6 and 0.65, respectively. Obtained values are lower than expected because the tables of calculated R_{ij} values correspond to an isolated N^{-3} anion.

The topology analysis of NaMgIm_3 has found that the underlying net is of the **stp** type. There are few MOFs with this topology type in the CSD database, and few inorganic compounds in the ICSD database. They all have a common structure type belonging to iron phosphonate $\text{Fe}_2(\text{HPO}_3)_3$. It is not a structural prototype of NaMgIm_3 , because the anion is different (phosphonate instead of imidazolate), and therefore, the space group is $\text{P6}_3/\text{m}$ instead of P6_322 . One more difference between NaMgIm_3 and Fe phosphonate is that in the latter two octahedral nodes are occupied by the same atom type (Fe).

CONCLUSION

In conclusion, it appears that the formation of AMgIm_3 compounds, where A is Li, Na and K, is governed by the thermodynamic stability of the alkali metal imidazolates versus the energy of formation of mixed metal imidazolate compounds; while lithium imidazolate does not react with magnesium imidazolate likely due to the limitation imposed by a small Li cation (A cations in AMgIm_3 have the coordination number 6), potassium imidazolate swiftly reacts with MgIm_2 and

forms KMgIm_3 . The double cation imidazolates of magnesium and sodium or potassium are the first members of new family of imidazolate frameworks with stp topology.

Acknowledgement. Authors acknowledge a financial support of Swiss National Science foundation in the scope of Joint research projects (SCOPEs) under the title: “Metal-Hydride Organic Frameworks (HOF) - new solids for gas adsorption and separation”. S.B. and J.P. acknowledge the financial support of Croatian Science Foundation in the scope of “*Development of early stage researchers carriers - education of new PhD students*”. This work was supported by FNRS (FRIA scholarship allocated to F.M., PDR T.0169.13, EQP U.N038.13, J.0164.17). The authors acknowledge the Swiss-Norwegian Beamlines of ESRF for the allocation of beamtime and excellent support with the data collection.

REFERENCES

1. Klebanoff, L. (Ed.), *Hydrogen Storage Technology: Materials and Applications*; Taylor & Francis: Florida, Boca Raton, 2013.
2. Paskevicius, M.; Jepsen, L. H.; Schouwink, P.; Černý, R.; Ravnsbæk, D. B.; Filinchuk, Y.; Dornheim, M.; Besenbacher, F.; Jensen, T. R. Metal borohydrides and derivatives - synthesis, structure and properties. *Chem. Soc. Rev.* 2017, *46*, 1565-1634.
3. Filinchuk, Y.; Richter, B.; Jensen, T. R.; Dmitriev, V.; Chernyshov, D.; Hagemann, H. Porous and dense $\text{Mg}(\text{BH}_4)_2$ frameworks: synthesis, stability and reversible absorption of guest species. *Angew. Chem. Int. Ed.* 2011, *50*, 11162-11166.
4. Rowsell, J. L.; Yaghi, O. M. Strategies for hydrogen storage in metal-organic frameworks. *Angew. Chem. Int. Ed.* 2005, *44*, 4670-4679.
5. Murray, L. J.; Dincă, M.; Long, J. R. Hydrogen storage in metal-organic frameworks. *Chem. Soc. Rev.*, 2009, *38*, 1294-1314.
6. Chen, B.; Ockwig, N. W.; Millward, A. R.; Contreras, D. S.; Yaghi, O. M. High H_2 adsorption in a microporous metal-organic framework with open metal sites. *Angew. Chem.* 2005, *117*, 4823-4827.
7. Filinchuk, Y.; Černý, R.; Hagemann, H. Insight into $\text{Mg}(\text{BH}_4)_2$ with Synchrotron X-ray Diffraction: Structure Revision, Crystal Chemistry, and Anomalous Thermal Expansion. *Chem. Mater.* 2009, *21*, 925-933.
8. Morelle, F.; Ban, V.; Filinchuk, Y. Towards hydridic nanoporous frameworks: the first imidazolate-borohydride compound Li_2ImBH_4 ($\text{Im}=[\text{C}_3\text{H}_3\text{N}_2]^-$). *Intl' symposium on metal-hydrogen systems (MH2014)*, Manchester, UK, July 20-25, 2014.

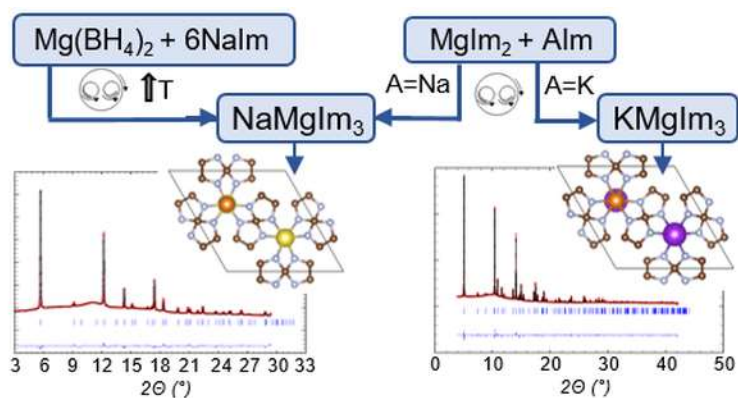
9. Park, K. S.; Ni, Z.; Côté, A. P.; Choi, J. Y.; Huang, R.; Uribe-Romo, F. J.; Chae, H. K.; O’Keeffe, M.; Yaghi, O. M. Exceptional chemical and thermal stability of zeolitic imidazolate frameworks. *Proc. Nat. Acad. Sci. USA* 2006, *103*, 10186.
10. Zhang, J.-P.; Zhang, Y.-B.; Lin, J.-B.; Chen, X.-M. Metal Azolate Frameworks: From Crystal Engineering to Functional Materials. *Chem. Rev.* 2012, *112*, 1001-1033.
11. Tian, Y.-Q.; Xu, H.-J.; Li, Y.-Z.; You, X.-Z. $[\text{Co}^{\text{II}}\text{Cu}^{\text{I}}_2(\text{Im})_4]_{\infty}$: A Layered Bimetallic Imidazolate Polymer, the First Hybridized Cobalt(II) Imidazolate. *Z. Anorg. Allg. Chem.* 2004, *630*, 1371.
12. Schubert, D. M.; Visi, M. Z.; Knobler, C. B. Acid-catalyzed synthesis of zinc imidazoles and related bimetallic metal-organic framework compounds. *Main Group Chem.* 2008, *7*, 311.
13. Graden, J. A.; Ellerby, L. M.; Roe, J. A.; Valentine, J. S. Role of Bridging Histidyl Imidazolate Ligands in Yeast Copper–Zinc Superoxide Dismutase. Characterization of the His63Ala Mutant. *J. Am. Chem. Soc.* 1994, *116*, 9743-9744.
14. Nguyen, N. T. T.; Lo, T. N. H.; Kim, J.; Nguyen, H. T. D.; Le, T. B.; Cordova, K. E.; Furukawa, H. Mixed-Metal Zeolitic Imidazolate Frameworks and their Selective Capture of Wet Carbon Dioxide over Methane. *Inorg. Chem.* 2016, *55*, 6201–6207.
15. Morelle, F. Hybrid hydridic frameworks by the combination of complex hydrides and nitrogen-based organic ligands. Ph.D. Dissertation, Univerité catholique de Louvain, Louvain-la-Neuve, Belgium, 2017.
16. Safin, D. A.; Robeyns, K.; Filinchuk, Y. Magnesium Imidazolate – a First Porous Zeolitic Imidazolate Framework with Alkali and Alkaline Earth Metals. *Acta Crystallogr., Sect. A: Found. Adv.* 2016, *72*, 402.
17. Bubble [Dyadkin, V., Pattison, Ph., Dmitriev, V., Chernyshov, D. *A new multipurpose diffractometer PILATUS@SNBL* [J. Synchrotron Rad., 23, 3, 2016](#)].
18. Favre-Nicolin, V.; Černý, R. FOX, "Free Objects for Crystallography": a modular approach to *ab initio* structure determination from powder diffraction. *J. Appl. Crystallogr.* 2002, *35*, 734-743.
19. Rodriguez-Carvajal, J. Recent advances in magnetic structure determination by neutron powder diffraction. *J. Physica B.* 1993, *192*, 55–69.
20. Blatov, V. A. Nanocluster analysis of intermetallic structures with the program package TOPOS. *Struct. Chem.* 2012, *23*, 955-963.
21. Brese, N. E.; O’Keeffe, M. Bond-Valence Parameters for Solids. *Acta Cryst.* 1991, *B47*, 192-197.

22. Momma, K.; Izumi, F. VESTA 3 for three-dimensional visualization of crystal, volumetric and morphology data. *J. Appl. Crystallogr.* 2011, 44, 1272-1276.

23. Burazer, S.; Guénée, L.; Robeyns, K.; Morelle, F.; Ban, V.; Popović, J.; Filinchuk, Y.; Černý, R. High temperature polymorph of NaIm. *In preparation.*

Supporting Information Available:

PXRD data of the S1 sample (Figure S1), PXRD data of the S2 sample, as prepared and thermally treated at 7220 °C (Figure S2), PXRD data of the S3 sample (Figure S3), PXRD data of Li sample (Figure S4). This material is available free of charge via the Internet at <http://pubs.acs.org>



Graphic: For table of contents only

Synopsis for table of contents: NaMgIm_3 and KMgIm_3 , first bimetallic imidazoles containing alkali and alkaline earth metals, are prepared by mechanochemical synthesis. *In-situ* high temperature XRPD experiment utilizing synchrotron radiation was used for structural evolution and thermal stability. Structures have been solved from synchrotron powder data. Both compounds crystallize in the $P6_322$ space group.